

EXAFS SPECTROSCOPY STUDY OF THE ATOMIC STRUCTURE OF ZnS NANOCOMPOSITE THIN FILMS

© R. G. Valeev,^{1,2} A. N. Beltukov,^{1,2} F. Z. Gilmutdinov,¹
É. A. Romanov,² A. N. Deev,¹ V. V. Kriventsov,³
N. A. Mezentsev,⁴ and A. I. Chukavin^{1,2}

UDC 538.9

The atomic structure of zinc sulfide films obtained by thermal evaporation in ultrahigh vacuum at condensation temperatures of –100°C, –50°C, and 0°C was investigated. Structural states were assessed by means of X-ray diffraction and atomic force microscopy. Fourier transform was used to study the local atomic environment and acquire the structural information (interatomic distances and coordination numbers) by zinc *K* edge EXAFS spectroscopy.

Keywords: ZnS, local atomic structure, EXAFS spectroscopy, X-ray diffraction, atomic force microscopy, Fourier transform, semiconductors, nanomaterials.

INTRODUCTION

Interest in the structure and properties of nanomaterials, which are widely used in optical applications, is related chiefly with manifestation of the size effects in physicochemical, optical and electronic properties. This made it possible to extend the application of base materials for semiconductor electronics and considerably reduce the size of individual elements, which is in line with the modern trend to miniaturization. This becomes topical for optoelectronics as well due to extended use of light pipes for information exchange between circuit elements, which requires both the light pipes and the data receipt-transfer units to be diminished in size [1, 2].

Zinc sulfide is a conventional material for the production of various optical devices and units, in particular, image formation systems (medical diagnostics, nondestructive testing of pieces, etc.), detection and radiometry systems, and IR lasers [3, 4]. Due to its high mechanical characteristics, chemical resistance and thermostability, zinc sulfide can be used both as individual material and in composites [5, 6].

Zinc sulfide films are conventionally prepared by gas-phase deposition and molecular beam epitaxy [7-9]. These methods have both the advantages (high structural perfection of the grown films, possibility of direct control of the structure and properties during the deposition) and drawbacks (high cost and long growth process). The possibility of using inexpensive and efficient method of powder material thermal evaporation (the flash method), which is characterized by a high deposition rate, is not sufficiently investigated. Of special interest is the film synthesis at low condensation temperatures. At the same time, it is very important in the film synthesis to control the functional properties, which are directly related to the following main factors: size, structure, shape and dispersion of nanoparticles, amount of structural defects, and uniform

¹Institute of Physics and Technology, Uralian Division, Russian Academy of Sciences, Izhevsk; valeev@lasas.fti.udm.ru. ²Udmurt State University, Izhevsk. ³G. K. Boreskov Institute of Catalysis, Siberian Division, Russian Academy of Sciences, Novosibirsk. ⁴G. I. Budker Institute of Nuclear Physics, Siberian Division, Russian Academy of Sciences, Novosibirsk. Translated from *Zhurnal Strukturnoi Khimii*, Vol. 52, Supplement, pp. S184-S188, 2011. Original article submitted October 15, 2010; revised April 11, 2011.

chemical composition. For example, even a small deviation in the length of interatomic bonds in semiconductors changes considerably the width of electron and hole zones and increases the total energy of optical transitions (blue and red shifts of absorption edge) [10].

In this connection, investigation of the local atomic structure, which parameters (chemical bond length, coordination number, root-mean-square deviations of atoms) can strongly depend on the conditions of film synthesis, should aid in understanding the formation of functional properties of zinc sulfide and extending the basic knowledge of their nature.

EXPERIMENTAL APPROACHES AND METHODS

ZnS films investigated in the present work were obtained by evaporation of powder material in ultrahigh (10^{-7} Pa) vacuum, which provided high chemical purity of the samples. The films ~150 nm in thickness were synthesized in a wide range of condensation temperatures (substrate temperatures). The films obtained at a substrate temperature of -150°C, -50°C and 0°C were chosen for further structural studies. The choice was related with the fact that thermal evaporation at low condensation temperatures was not used earlier for the film synthesis; structure and functional properties of such films were not studied. Quartz was chosen as a substrate, because it is X-ray amorphous and does not give additional reflections in diffraction patterns, in distinction to crystalline silicon used in our previous works. The film stoichiometry and content of admixtures (carbon and oxygen, their presence in unbound state in subsurface layers having no effect on electrophysical and optical properties) were controlled by electron spectroscopy for chemical analysis (ESCA) on an ES-2401 X-ray emission spectrometer at the Institute of Physics and Technology, Uralian Division, Russian Academy of Sciences, Izhevsk. Surface morphology was examined by atomic force microscopy (AFM) on a Solver (NT-MDT) atomic force microscope at the Udmurt State University (UdSU), Izhevsk. X-ray diffraction studies were performed on a DRON-6 diffractometer (UdSU).

For all the samples, Zn *K* edge EXAFS spectra were recorded from the fluorescence yield on an EXAFS spectrometer at the Siberian Synchrotron Radiation Center (8th channel, SSRC, Novosibirsk, Russia). The VEPP-3 storage ring with the electron beam energy 2 GeV at average current 80 mA was used as a source of X-ray radiation. Radiation was monochromated using a single-unit slotted Si(111) crystal monochromator. EXAFS spectra were recorded at the Zn *K* edge ($E_K = 9\,659$ eV, energy scanning range 9550-10450 eV, step 1.5 eV).

X-ray emission was recorded using ionization chambers and a detector (photomultiplier tube + luminophor). The oscillating part $\chi(k)$ was distinguished by a standard technique [11]. Fourier transform module $k^3\chi(k)$ over the wave number range 3.0-13.0 Å⁻¹ was used to obtain the radial distribution function of atoms (RDF). Structural information, i.e., distances, coordination numbers and Debye factors, was acquired by modeling the spectra (the fitting procedure) with the Viper software [12, 13] after Fourier filtration using the literature XRD data for reference compounds.

RESULTS AND DISCUSSION

To analyze the chemical composition of ZnS films, survey spectra were recorded for each sample, C1s, O1s, S2p, and Zn2p_{3/2} spectra were studied in detail. The spectra were excited by MgK_α radiation ($E = 1253.6$ eV). To clean the surface from adsorbed impurities and remove the ~10 nm surface layer with a distorted composition, etching with Ar⁺ ions at the energy of 0.9 keV and current density 12 mKA/cm² was employed.

The study showed that the free surface has adsorbed hydrocarbon impurities and adsorbed oxygen. Impurities are completely absent for 10 min after etching. Oxygen is present in small amounts; however, as it is not chemically bound to zinc with the formation of ZnO, it has no effect on electrophysical characteristics of the films.

The concentration ratio of sulfur and zinc before and after ionic etching is presented in Table 1. The binding energies for S2p line correspond to its metal compounds. E_b for Zn2p_{3/2} line is within the limits characteristic of Zn-S compounds. However, it should be noted that the concentration ratio of Zn and S somewhat differs from the ratio typical of the stoichiometric ZnS compound.

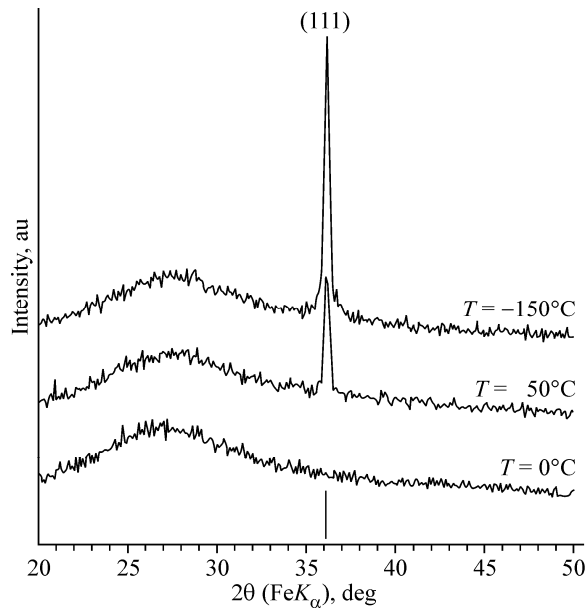


Fig. 1. X-ray diffraction patterns of zinc selenide films.

TABLE 1. Concentration of Elements in ZnS Films, at.%

Sample temperature, °C	Etching, min	C	O	S	Zn
0	0	47.8	21.9	22.6	7.8
	10	0	2.8	56.2	40.1
-50	0	53.3	21.0	17.6	8.1
	10	0	4.3	54.9	40.9
-150	0	72.8	22.9	0.0	4.4
	10	0	6.9	48.3	44.9

According to X-ray diffraction data illustrated in Fig. 1, intensity of the first peak (111) grows as the condensation temperature decreases, which indicates an increase of the X-ray emission coherent scattering units and hence the size of film grains. An amorphous halo is observed in the angle region of 27°, which appearance is related with the contribution from amorphous phase of the material to diffraction pattern. Position of the reflection corresponds to the structure of bulk cubic CdS.

Fig. 2 displays AFM images of the film surface obtained on the silicon substrates. The oriented growth of conic islets with nanometer height (the so-called “nanoobjects”) is seen to occur on the film surface. The nanoobjects are oriented in one direction irrespective of the substrate type and condensation temperature.

In the EXAFS experiment, the ZnK edge X-ray absorption spectra ($E_K = 9659$ eV, energy scanning region 12550–13500 eV, step 1.5 eV) were obtained. The sulfur K edge spectra were not taken due to energy limitations of VEPP-3 (the sulfur K edge is in the region of “mild” X-ray radiation and cannot be recorded). The normalized oscillating parts of the spectra after standard pretreatment along with their Fourier images are depicted in Fig. 3 and compared with the model ones calculated using the FEFF-8 software [14]. Table 2 lists parameters of the local environment of zinc atoms calculated by the Fourier transform method with fitting by the Viper software [12, 13].

A detailed analysis of the features and shape of Fourier images and structural data listed in Table 2 allows a conclusion that radii of the first coordination spheres (Zn–S pairs) within the processing error are independent of the condensation temperature upon sputtering and coincide with the data obtained for crystalline ZnS. This fact may be related to a higher ionicity of chemical bonds between sulfur and zinc atoms in the studied systems.

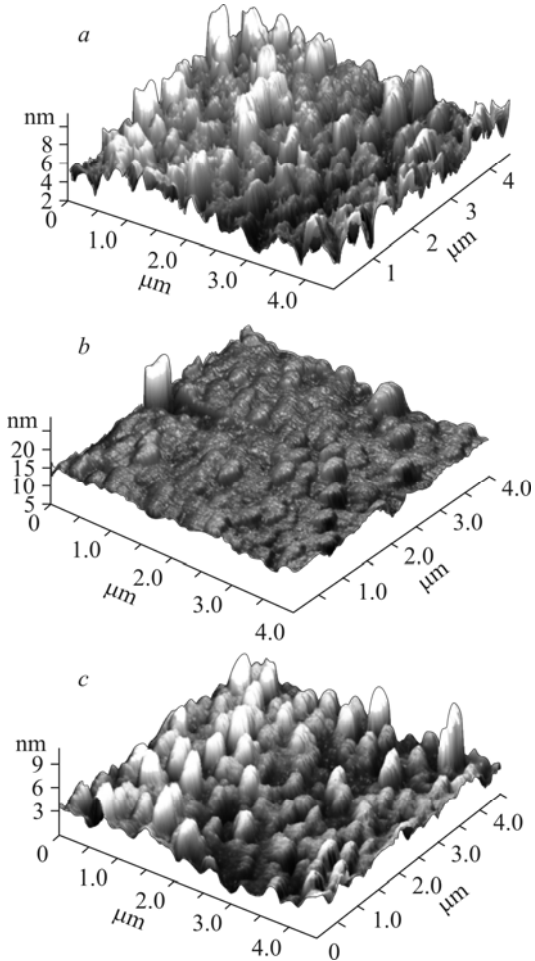


Fig. 2. AFM images of ZnS film surfaces: condensation temperature -150°C (a), condensation temperature -50°C (b), condensation temperature 0°C (c).

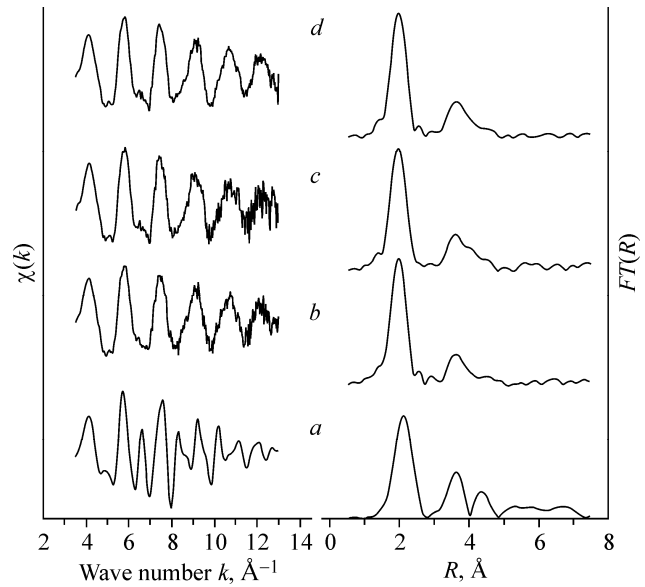


Fig. 3. Normalized oscillating parts of EXAFS spectra for the films and their Fourier images: model (a), condensation temperature -150°C (b), condensation temperature -50°C (c), condensation temperature 0°C (d).

TABLE 2. Parameters of Zinc Atom Local Environment

Condensation temperature, $^{\circ}\text{C}$	$R_1, \text{\AA}$	N_1	$R_2, \text{\AA}$
Model	2.338	4.0	3.818
-150	2.33(2)	3.3(4)	3.93(5)
-50	2.33(2)	3.9(4)	3.93(5)
0	2.34(2)	3.8(4)	3.90(5)

Note. R_1 and R_2 are interatomic distances to the 1st and 2nd coordination spheres; N_1 is the coordination number in the first coordination sphere.

Coordination numbers in the first coordination sphere for the samples sputtered at the substrate temperatures 0°C and -50°C are close to crystallographic values. Note that the S:Zn concentration ratio increases with the condensation temperature (Table 1). This underlies a decrease in respective coordination number for the sample sputtered at the substrate temperature of -150°C .

The average position of atoms in the second coordination sphere (Zn-Zn) is shifted toward higher values by 0.1\AA (to 3.93\AA as compared with 3.82\AA in the bulk sulfide). As the diffraction data testify to the presence of bulk ZnS where the

Zn–Zn distance is equal to 3.82 Å, the difference between XRD and EXAFS data indicates that in the presence of large particles a greater part of zinc resides in small particles, which are not detected by XRD; such particles have a distorted, probably amorphous structure. Structural distortions lead to disordering of Zn–Zn interatomic distances. The Zn–S distances do not change because their length is related primarily with the chemical bond length rather than with morphology of the sulfide. The next Zn–S distance (the third coordination sphere) is not observed probably due to a wide spread of distances in the distorted structure. Structural state of the studied films can be considered as a composite represented by nanocrystals in amorphous matrix of the material.

This work was financially supported by the RAS Presidium Programs Nos. 20 (Project 09-P-2-1026), 21 and 27, Innovation Program for Young Scientists UD RAS, RF President's Grant (Agreement No. 02.120.11.369-MK), Rosnauka Contract No. 02.740.11.0543, and Russian Foundation for Basic Research (Project No. 11-03-01264).

REFERENCES

1. H. Babucke, P. Thiele, T. Prasse, et al., *Semiconductor Science and Technology*, **13**, 200 (1998).
2. M. Strasburg, I. L. Krestnikov, Z. I. Alferov, et al., *Physica E*, **2**, 542 (1998).
3. S. Itoh, K. Nakano, and A. Ishibashi, *J. Crystal Growth*, **214/215**, 1029 (2000).
4. M.-C. Jeong, B.-Y. Oh, M.-H. Ham, et al., *Appl. Phys. Lett.*, **88**, 202105 (2006).
5. Y. Wang, Z. Liu, B. Han, et al., *Chem. Phys. Lett.*, **381**, 271 (2003).
6. L. Yankuan, X. Guangcheng, C. Shaofeng, et al., *Nanotechnology*, **18**, 285605 (2007).
7. I. P. Kalinkin, V. B. Aleskovskii, and A. V. Simashkevich, *Epitaxial Films of A^2B^6 Compounds*, Zhdanov LSU, Leningrad (1978).
8. S. A. Kukushkin and A. V. Osipov, *UFN*, **168**, No. 10, 1083 (1998).
9. A. P. Belyaev, V. P. Rubets, and I. P. Kalinkin, *Phys. Solid State*, **39**, No. 2, 382 (1997).
10. Jiming Bao, Mariano A. Zimmler, Federico Capasso, et al., *Nano Lett.*, **6**, 1719 (2006).
11. R. G. Valeev, D. V. Surnin, A. N. Beltukov, et al., *J. Struct. Chem.*, **51**, Supplement, S132 (2010).
12. K. V. Klementiev, <http://www.desy.de/~klmn/viper.html>.
13. K. V. Klementiev, *J. Phys. D: Appl. Phys.*, **34**, 209 (2001).
14. S. I. Zabinsky, J. J. Rehr, A. Ankudinov, et al., *Phys. Rev. B*, **52**, 2995 (1995).